Supplementary Table 1 | DMI vectors. The site information, distance (in Å), DMI vector (in meV), DMI strength (in meV) and D/J (J is the Heisenberg exchange) of the six inequivalent exchange paths.

Path	Site information	Distance	D_x	D_y	D_z	$\|D\|$	$\|D/J\|$
I	8*c*-8*c*	2.295	0.01	1.00	0.05	1.00	0.044
II	8*c*-12*d*	2.559	-4.36	-4.35	-4.87	7.85	0.854
III	8*c*-12*d*	2.556	-1.03	-1.29	-1.30	2.10	0.278
IV	8*c*-12*d*	2.430	-1.26	-0.65	-1.22	1.87	0.103
V	12*d*-12*d*	2.517	3.91	3.37	2.93	5.94	0.417
VI	12*d*-12*d*	2.613	-1.58	-1.21	-1.86	2.72	0.354

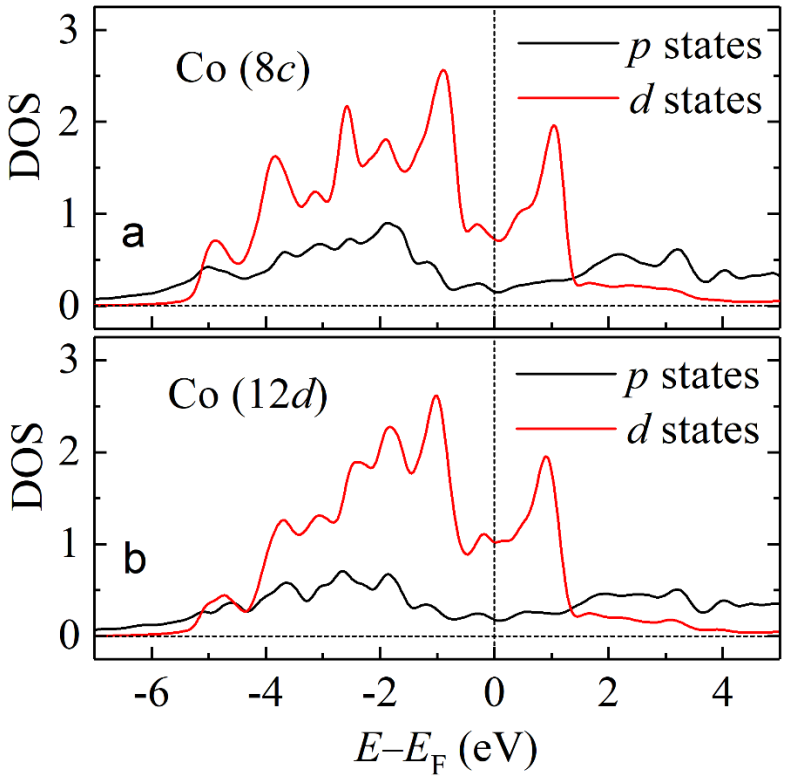

Supplementary Figure 1 | Density of states. The total density of states (DOS) of *p* and *d* orbitals for Co(8*c*) (**a**) and Co(12*d*) (**b**). The DOS-*p* has been amplified by ten times for a better view. E_F is the Fermi level.

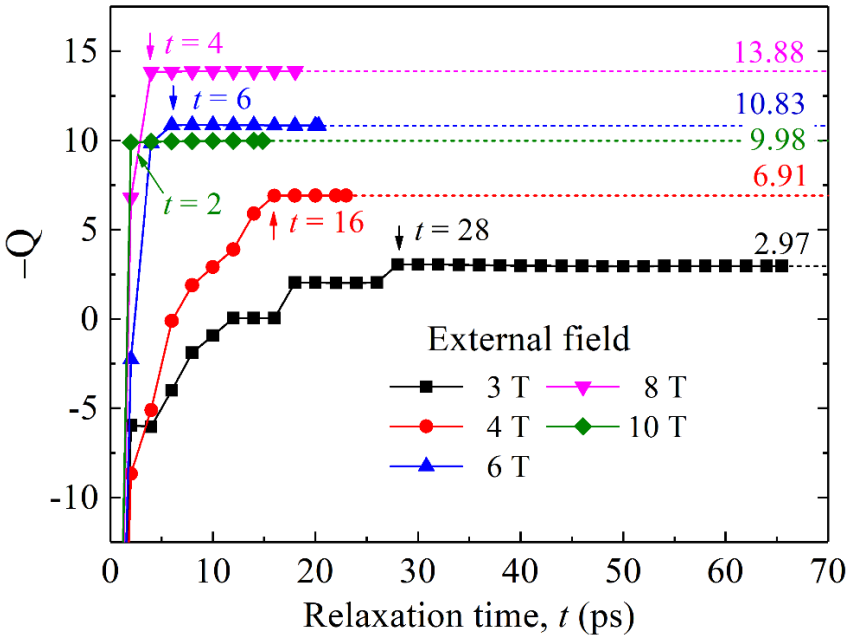

Supplementary Figure 2 | Topological charge. The time evolution of topological charge under external fields from 3 to 10 T. The arrows point out when the topological charge is stabilized. The dashed lines represent expected stable −Q for longer relaxation time.

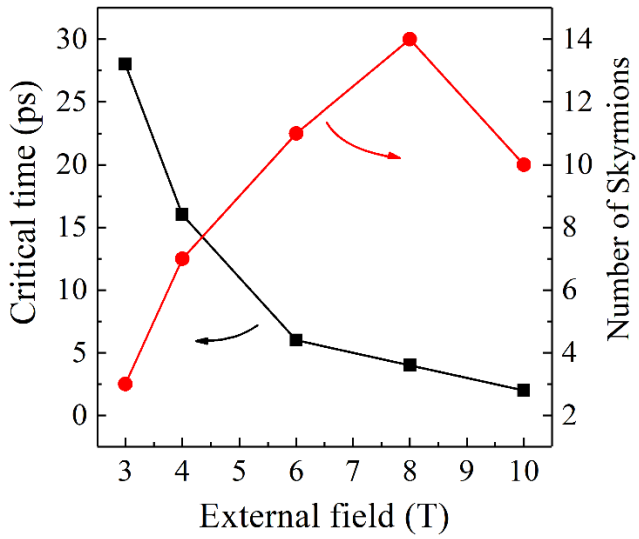

Supplementary Figure 3 | Critical time and number of skyrmions. The critical time needed to stabilize the skyrmions and the number of skyrmions obtained in the simulation under different external fields.

Supplementary Note 1 | DMI and electronic structure. The DMIs are calculated by using the energy mapping technique developed by Xiang *et al.*[1] by assuming that the generalized 3×3 exchange matrix [**J**] is antisymmetric[2] so that $\mathbf{D} = (J_{yz}, J_{zx}, J_{xy})$. Here, we list the DMI vectors and related information in Supplementary Table 1 for the six inequivalent exchange paths depicted in Fig. 1 in the main text. It can be seen that the DMIs for path II and V are remarkably strong, while other ones are much weaker. To verify the assumption, we also calculated the full [**J**] using the same technique for path II and V. The obtained **D** is $-(4.26, 4.27, 4.74)$ meV and $(3.80, 3.30, 2.86)$ meV for path II and path V, respectively, which are very close to the corresponding ones in Table 1.

Assuming that Moriya's theory[3] applies to the case here, the DMI is given by a sum of different three-hopping processes between two atoms in the presence of SOC. The SOC strength is a constant (15.5 meV). Our calculation shows close spin moments of 1.66 and 1.76 μ_B for Co(8*c*) and Co(12*d*), respectively. The orbital moment is about 0.065 μ_B for both sites. Hence, the difference in hopping can be expected to dominate the variation of DMI.[3] A three-hopping process may be described in this way: an electron hops to an unoccupied state due to SOC, then the resulting hole hops to the occupied state of the neighboring atom and hops back finally to the unoccupied state of the original atom. As shown in the main text, the hopping magnitudes for path II and V are exceptionally strong. In particular, the hopping that involves *p* orbitals is much stronger than other ones without *p* orbitals.

In order to explore the physics behind the strong hopping in path II and V, we plot the total density of states (DOS) of *p* and *d* orbitals for both Co(8*c*) and Co(12*d*) sites in Supplementary Fig. 1. For both sites, an unoccupied *d* peak is shown in the DOS right above the Fermi level. It is clear that *p* and *d* orbitals strongly hybridize with each other in the occupied states. DOS-*p* has a larger energy span than DOS-*d*, indicating a farther spatial extension of wave functions that facilitates the hopping. Hence, it is expected that, after the mixing between occupied and unoccupied *d* states (contributed almost equally by all decomposed *d* orbitals) due to SOC, the resulting hole has both *p* and *d* characters and can hop to the occupied *p* or *d* states of the neighboring atoms due to large *p*–*p* and *p*–*d* hopping. Finally, the hole hops back to the unoccupied *d* states of the original atom due to a large

p–d and *d–d* hopping. It is worth mentioning that the decomposed orbitals extending toward each other generally have stronger hopping due to a larger overlap of wave functions according to the calculation.

Supplementary Note 2 | Topological charge. To investigate the evolution of skyrmions from randomized spin configurations, we calculate the topological charge varying with simulation time. Instead of using the original definition of $Q = \frac{1}{4\pi}\int d^2r\mathbf{S}\cdot(\partial_x\mathbf{S}\times\partial_y\mathbf{S})$, the lattice version of topological charge[4] is adopted since it was recently shown to better capture the dynamical process of topological transition.[5] To construct the lattice model, the spin configuration is divided by a 200×200 square mesh and the magnetic moment of each mesh point is calculated by averaging the surrounding moments when their *x* and *y* coordinates fall into a lattice square. This is a reasonable choice because the moments do not rotate much relatively in a lattice square regarding that the square length is small (0.5*a*) compared to the spiral period (30*a*). Each skyrmion contributes −1 to the topological charge in this case. The −Q thus corresponds to the generated number of skyrmions (within small model errors) if skyrmions are the only non-collinear configurations in the pattern, as shown in Supplementary Fig. 2. As the external field increases, the stabilized −Q increases from 2.97 (~3) at 3 T to 13.88 (~14) at 8 T and then decreases to 9.98 (~10) at 10 T. These results are well consistent with the number of skyrmions shown in the magnetic patterns. A higher external field stabilizes the topological charge faster. The critical time decreases rapidly from 28 to 2 ps when the external field increases from 3 to 10 T as shown in Supplementary Fig. 3. This is because the speed of spin realignment from a randomized configuration is accelerated by Zeeman effect under a higher external field while it is relatively slow when the magnetic pattern is a result of the compromise between Heisenberg exchange and DMI under a low external field. A fast realignment of moments by a higher external field also preserves more nuclei that can evolve into skyrmions until the field is so high that polarizes the spin textures.

Supplementary references

1. Xiang, H.J., Kan, E.J., Wei, S.-H., Whangbo, M.H. & Gong, X.G. Predicting the spin-lattice order of frustrated systems from first principles. *Phys. Rev. B* **84**, 224429 (2011).
2. Xu, C., Xu, B., Dupé, B. & Bellaiche, L. Magnetic Interactions in BiFeO3: a First-Principles Study. Preprint at *arXiv:1811.09574* (2018).
3. Moriya, T. Anisotropic Superexchange Interaction and Weak Ferromagnetism. *Phys. Rev.* **120**, 91-98 (1960).
4. Berg, B. & Lüscher, M. Definition and statistical distributions of a topological number in the lattice O(3) σ-model. *Nucl. Phys. B* **190**, 412-424 (1981).
5. Yin, G. et al. Topological charge analysis of ultrafast single skyrmion creation. *Phys. Rev. B* **93**, 174403 (2016).